Proceedings of the Combustion Institute 40 (2024) 105683

Contents lists available at ScienceDirect

Proceedings of the Combustion Institute

journal homepage: www.elsevier.com/locate/proci

N_2O oxidized combustion of ethylene: Detailed laminar flame structure and the significance of oxidizer decomposition kinetics for modeling

Martin Hoener [a], Thomas Bierkandt [b], Shkelqim Shaqiri [a], Tina Kasper [a,*]

[a] Technical Thermodynamics, Paderborn University, Paderborn, Germany
[b] Institute of Combustion Technology, German Aerospace Center (DLR), Stuttgart, Germany

ARTICLE INFO

Keywords:
N_2O
HCNO
HNCO
Laminar flame
PEPICO

ABSTRACT

We report the detailed flame structure of an N_2O oxidized, fuel-rich flame of ethylene (C_2H_4) at an equivalence ratio of 1.2, measured with double-imaging photoelectron photoion coincidence spectroscopy (i^2PEPICO) using synchrotron vacuum ultraviolet photoionization. We analyze the oxidizer decomposition and the intermediate chemistry with a focus on isomer branching ratios of CHNO and on the abundantly produced HCN (hydrogen cyanide). A detailed mechanism is composed that comprises recently reported reaction rates for N_2O decomposition and detailed hydrocarbon chemistry and nitrogen chemistry. The new mechanism is based on the Aramco 3.0 chemistry set. The predictive accuracy for both main species mole fractions and intermediate mole fractions, was significantly improved. The mechanism shows excellent agreement with the flame measurements and improves upon existing mechanisms. As a first, we were able to detect, separate and assign the signals of two of the CHNO isomers and tentatively assign an isomer branching ratio to HCNO (fulminic acid) and HNCO (isocyanic acid). H radicals show significant activity throughout the whole reaction network in the provided analysis. They interact in the decomposition of the fuel and act as a driver of intermediate formation and destruction. The presented data is a first detailed look at the fuel and oxidizer decomposition for these flames using synchrotron photoionization methods and delivers valuable data for the development and validation of chemical kinetics mechanisms. We conclude that the decomposition kinetics of N_2O play a significant role in the remaining kinetics of the combustion process under the reported flame conditions and influence the whole reaction network down to intermediate species.

1. Introduction

Nitrous oxide (N_2O) plays an important role in combustion processes both as an intermediate and as an oxidizer. One of the pathways to produce oxides of nitrogen in air oxidized flames involves N_2O [1]. Under those reaction conditions, the oxygen radical can attack the molecular nitrogen supplied by the air.

Liquefied mixtures of hydrocarbons and N_2O are considered as a green propellant alternative to classical nitrogen-based propellants such as hydrazine-based fuel compounds [2]. A premixed green propellant currently under investigation is based on an ethylene (C_2H_4) and N_2O blend [3]. Premixed green propellants are advantageous, because they consist of non-toxic components and are non-toxic themselves. Because of premixing of the fuel and oxidizer, the resulting liquid monopropellant can be stored in a single tank and delivered to rocket propulsion systems using a monopropellant feed, with the associated low component count and light weight. N_2O has a relatively high vapor pressure, which enables (partial) self-pressurization of the monopropellant mix [4].

The use in advanced space propulsion technologies and its role in air oxidized combustion makes an understanding of N_2O decomposition and interaction with hydrocarbons in combustion systems imperative.

Several flames of N_2O oxidized hydrocarbons and other fuels have been investigated. Early work on premixed N_2O/acetylene flames was performed by Darian and Vanpee [5]. They used spectroscopic techniques to gain understanding of rich and lean flames and found that the combustion takes place in two steps, with the decomposition of N_2O into O_2, N_2 and NO preceding the subsequent combustion of the fuel with the released oxygen.

Powell and Papas provide similar data for N_2 diluted stoichiometric hydrocarbon flames of CH_4, C_2H_2 and C_3H_8 at a pressure of 0.81 bar [6]. Through sensitivity analysis they found the highest sensitivity of results

* Corresponding author.
E-mail address: tina.kasper@uni-paderborn.de (T. Kasper).

https://doi.org/10.1016/j.proci.2024.105683
Received 3 December 2023; Accepted 21 July 2024
Available online 19 August 2024

depends on N_xH_y concentrations and more specifically the imidogen radical (NH). Work by Allen et al. also suggests significance of N_xH_y species in N_2O oxidized combustion, albeit their work investigated hydrogen nitrous oxide systems [7]. In preceding work the same authors investigated N_2O oxidized combustion of hydrogen [8].

A detailed flame structure is available for an argon-diluted CH_4/N_2O flat flame published by Vandooren et al. [9]. This stoichiometric flame was investigated by molecular-beam quadrupole mass spectrometry utilizing electron ionization. Results were compared to an argon-diluted CH_4/O_2 flame. The authors successfully identified NCO, HCN, and HNCO as important species arising from nitrogen fuel interactions. A flame with similar conditions involving CH_4 and N_2O was investigated by Zabarnic using laser-induced fluorescence (LIF) and compared to a NO-doped CH_4/O_2 flame and modeled by a multi-step kinetics mechanism [10].

Several studies investigate N_2O oxidized flames, without the addition of hydrocarbons, e.g. in N_2O/H_2 systems and flames of ammonia oxidized with N_2O [11–15]. Vandooren et al. added CO to the reactant mix in a study investigating $H_2/CO/N_2O$ flames and found that CO only shows minor interaction with the N_2O oxidizer and does not have a significant role in oxidizer decomposition. A similar observation was made for CO/N_2O flames at different rich conditions by Dindi et al., who found that such flames completely lack any reactive radicals except for atomic oxygen [15].

Recent work by Wang and Zhang is aimed at understanding flame speeds in N_2O oxidized combustion of ethylene (C_2H_4) [16]. Work by Werling et al. concentrates on investigation of flame propagation with an emphasis specifically on the flashback characteristics of C_2H_4 combusted with N_2O in rocket propulsion applications [17].

Recent further advances have been made in understanding the decomposition kinetics of N_2O by Janzer et al. who published a set of corrected reaction rates for the decomposition of N_2O in hydrocarbon fuel systems, validated against flame speed measurements [3].

The goal of this work is to understand the interactions of N_2O as an oxidizer with hydrocarbon fuels and to improve the modeling of such oxidizer hydrocarbon systems. This work is motivated by advances in space propulsion, the possibility to use nitrogen compounds in carbon-free combustion processes and the wide use of N_2O in combustion processes, e.g. to increase performance in reciprocating engines.

2. Experimental and simulation

In this work, we investigate an N_2O oxidized flame of ethylene (C_2H_4) at an equivalence ratio of 1.2 with respect to the oxygen content of the N_2O oxidizer. The flame was stabilized on a McKenna type burner with a diameter of 60 mm at 60 mbar and a total flow rate of 4 slm. To act as an inert reference for data analysis and to lower the very high combustion temperatures, due to the energy release during N_2O decomposition, the flame was diluted with 25% argon. The flame was analyzed with the CRF-PEPICO endstation at the Swiss Light Source [18]. Measurements were performed with double-imaging photoelectron photoion coincidence spectroscopy. Direct samples from the flame are ionized with synchrotron vacuum ultraviolet light. Measurements are performed in a spatially resolved manner by varying the height of the sampling point with respect to the burner surface (HAB). Details of the experiment setup and data evaluation procedure can be found in [19]. Determined mole fraction profiles of all identified species can be found in the Supporting Information (SI) and will serve as validation data for the development of reaction mechanisms.

The exhaust gas temperature was measured utilizing the same experimental chamber used with the CRF-PEPICO endstation by means of a SiO_2 coated platinum-rhodium thermocouple. The sampling rate (i.e., flow of gas through the sampling nozzle orifice) is dependent upon the flame temperature at the point of sampling. The temperature translates to different spectrometer chamber pressures, which can be used to determine the temperature profile. The perturbed flame temperature profile was calculated using the method described by Struckmeier et al. [20]. Their approach considers the temperature disturbance created by the sampling probe and relates the radiation corrected exhaust gas temperature to the measured pressure profile of the flame. The profile was smoothed to remove steps occurring due to the course sampling grid at higher heights above burner (cf. Fig. 2).

A new detailed reaction mechanism containing C/H/O and nitrogen chemistry is composed. First, the base mechanism includes the full set of C/H/O chemistry from the Aramco 3.0 mechanism [21] and the nitrogen chemistry subset from Glarborg et al. [1] and is denoted M1. Second, this base mechanism is enhanced with reaction rates for N_2O decomposition published by Janzer et al. [3] and denoted M2. Both mechanisms contain the same reactions. In M2, only the reaction rates for R1, R2 and R3 have been updated by the rates proposed by Janzer et al. to improve the understanding of the influence of N_2O decomposition rates, the base mechanism (M1) and the enhanced mechanism (M2) are compared and validated against the measured N_2O-oxidized ethylene flame data. The enhanced mechanism shows a generally improved agreement with the experimental data across several species as we will demonstrate in the following sections. A direct comparison of the base mechanism M1 to the enhanced mechanism M2 is sought in the figures displayed in the present work. Both the M1 and M2 mechanisms are included in the Supporting Information. Simulations were performed with the laminar flame model of Ansys Chemkin 2023 R2 and the Cantera flame reactor module for burner-stabilized flames of Kintech Lab Chemical Workbench (Version 4.1.19528, 2017). Both simulation packages yielded identical results.

3. Main species and N_2O decomposition kinetics

The bright purple flame (Fig. 1) shows a relatively wide reaction zone from the pre-heat zone to completion of oxidizer decomposition. The measured temperature profile (top panel) and the experimental main species profiles compared to the simulation results of mechanisms M1 (center panel) and M2 (bottom panel) are shown in Fig. 2. It can be seen that the temperature rises steeply up to ca. 5 mm HAB corresponding to an almost complete destruction of the N_2O oxidizer. The temperature profile then shows a distinct plateau, in a region where the remaining N_2O is consumed reaching temperatures in excess of 2000 K to then decrease to the exhaust gas temperature. The measured mole fraction profiles show that the decline in fuel concentration precedes the N_2O decomposition and the fuel is completely consumed at a HAB of ca. 4.25 mm, where ca. 26% of the initial N_2O concentration persists. N_2O is only completely consumed at a HAB of 6.25 mm.

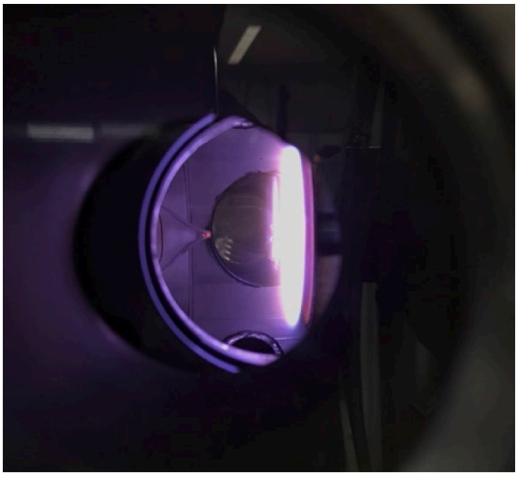

Fig. 1. Photograph of the argon-diluted C_2H_4/N_2O flame in the PEPICO flame chamber during measurements with the CRF-PEPICO endstation at the Swiss Light Source.

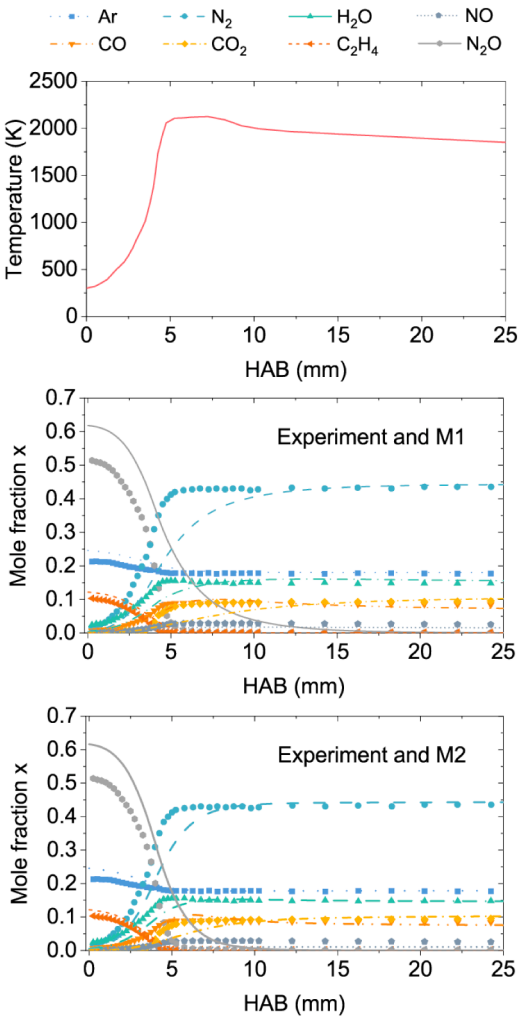

Fig. 2. Temperature profile of the flame (top panel) and the experimental mole fraction profiles of major species in comparison to results of M1 (center panel) and M2 (bottom panel). Measurements are shown as symbols, while the mechanism results are shown as lines.

The systematic difference in the species concentrations may mostly be attributed to quantification errors in the mole fractions obtained by element balancing. Some error may also be attributed to the resolution of convolution in the mass spectra. These isobaric convolutions had to be resolved by signal subtraction procedures. The resolution was possible due to the synchrotron photoionization method used in the experiments [19].

N_2O decomposition, albeit exothermal, is a slow process. While Wang and Zhang [16] incorrectly state that this can be attributed to endothermic decomposition of N_2O, the correct explanation for this behavior is the abnormally slow decomposition characteristics of N_2O [22] due to its energetics. This slow decomposition behavior may be attributed to the *spin-forbidden nature* [22] of the rather intuitive unimolecular N_2O decomposition to form N_2 and O* according to R1. The direct decomposition to N_2 and atomic oxygen would require a spin-forbidden transition to arrive at the triplet state of atomic oxygen from a singlet N_2O [22] and is kinetically unfavorable.

In spin-allowed processes, initial decomposition progresses through R2 and R3 [3].

$$N_2O+(M) = N_2+O+(M) \quad (R1)$$

$$N_2O+H = N_2+OH \quad (R2)$$

$$N_2O+H = NO+NH \quad (R3)$$

These two reactions are thus kinetically more favorable, but they require the presence of atomic hydrogen, which is provided by fuel decomposition.

This circumstance is clearly visible when the spatial distributions of N_2O and H in the flame are compared as displayed in Fig. 3. While substantial concentrations of the N_2O oxidizer are still present in the flame, the H radical concentration remains below the very sensitive [23] detection threshold. The increase in H concentration only takes place after a HAB of almost 5 mm, where the temperature plateau begins, and the oxidizer is almost completely consumed.

Insight into the reaction network has been gained using rate of production (ROP) analyses of M2. Fig. 4 shows a relative rate of production analysis concerning the destruction of the N_2O oxidizer in the flame in presence of fuel (i.e., 3.5 mm HAB) and in the post flame zone (i.e., 6.5 mm HAB), where the fuel is completely consumed.

A complete ROP analysis with respect to the nitrogen flow at 3.5 mm HAB and over the entire flame is included in the SI (cf. Figs. S2 and S4). In the flame zone, H is mainly produced by the reaction of CH_2 with CH_3 according to R4 to form ethylene and hydrogen atoms (cf. Fig. S1). A plethora of other reactions of H_2 with hydrocarbons also produces H in this zone (cf. Figs. S1 and S3). The reaction of N_2O with carbon monoxide (R5), albeit present at a substantial concentration in the flame, shows a negligible impact in the modeled reaction network.

The observation that CO does not interact with N_2O is corroborated by the findings reported by Vandoren and Tiggelen and Dindi et al. that little interaction between CO and N_2O exists in N_2O decomposition processes [12,15].

The main reaction consuming N_2O in the flame zone at increasing temperature is R2. In this zone, the unimolecular reaction R1 has a negligible role in N_2O destruction. The OH produced by R2 in turn reacts with molecular hydrogen to form water and H ($OH + H_2 = H_2O + H$), further driving N_2O decomposition.

R3 at a substantial backward rate acts to regenerate N_2O consuming NO and NH at lower HABs in the pre-heating zone of the flame.

$$CH_2+CH_3=C_2H_4+H \quad (R4)$$

$$N_2O+CO=CO_2+N_2 \quad (R5)$$

NO production thus may not depend on the primary decomposition of N_2O but on subsequent reactions with intermediates.

Some of the NO for example, is produced in a reaction sequence starting by CH attacking N_2 to yield NCN, a well-known reaction taking place in prompt NO formation [24]. In a similar fashion CH can attack N_2O to form NO and HCN.

The hot zone beyond 5 mm HAB shows a different picture as is displayed in the right panel of Fig. 4. Here, the kinetically unfavorable unimolecular decomposition according to R1 can take place at a higher rate, and a substantial fraction of ca. 30% of the total nitrogen flow can be attributed to this reaction. This behavior may also be attributed to the deprivation of H from fuel decomposition reactions in this zone.

These results are in excellent agreement with the sensitivity analyses

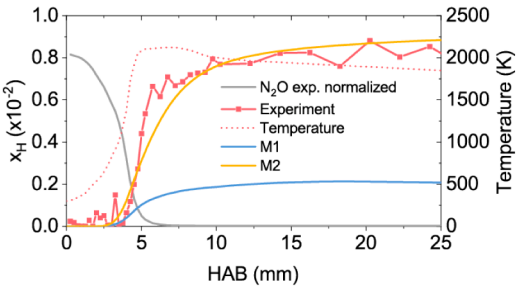

Fig. 3. H atom mole fraction profiles compared to the measured N_2O profile. The experimentally determined N_2O profile is renormalized to the maximum H concentration (denoted N_2O exp. normalized in the legend).

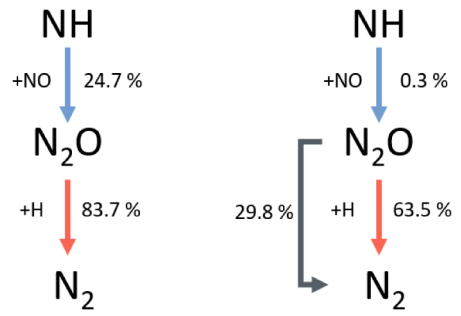

Fig. 4. A ROP analysis of N_2O decomposition reactions with respect to total N flow at 3.5 mm HAB (left) and 6.5 mm HAB (right).

reported by Janzer et al. They found that in N_2O oxidized flames of C_2H_4, R2 and R3 show the greatest sensitivities [3].

Reactions R1, R2 and R3 are the ones which were optimized by Janzer et al. [3] and incorporated in the M2 model in the present work. M1 contains the previously published reaction rates used by Glarborg et al. [1]. Their significant influence on the overall reaction network and the positive impact of the optimized rates reported by Janzer et al. on model performance is visible in Fig. 2. It can be seen that the agreement of the modeled major species profiles with the measurements is improved. Most significantly, predictions of oxidizer and fuel decomposition are both improved in M2. The modeled N_2O profile declines more steeply, similar to the measured data and shows complete consumption at significantly lower HABs than M1. Furthermore, M1 suggests a much slower decomposition at higher temperatures and, therefore, a shallower slope in the N_2O profile. The decline of the oxidizer is mirrored by the rise in molecular nitrogen concentration, a main decomposition product of the oxidizer as discussed before. The N_2 mole fraction profile shows significant improvement in its modeled progression with M2. The improved predictive capability of the M2 model with respect to fuel and oxidizer decomposition shows the importance of N_2O decomposition rates on model performance.

Both mechanisms underestimate the N_2O decomposition in the measured data. While with M1 the decline takes place up to a HAB of 15 mm, the N_2O is predicted to be destroyed completely at a HAB of 7.5 mm by M2. This value is much closer to the measured HAB of 6.25 mm for complete N_2O destruction. Therefore, no N_2O stemming from the fresh gas is available to the modeled reaction above a HAB of 7.5 mm which significantly influences the remaining reaction network with the improved M2 mechanism. So, in conclusion it can be said that the N_2O decomposition is predicted to be substantially more rapid with the improved model M2, which is a significant result and a substantial improvement of the predictive capability of M2 over M1 as this much more closely reflects the measurement. Since N_2 is the main decomposition product of N_2O, the N_2 profile mirrors the underestimated N_2O decline and N_2 rises much more steeply in the measured data than in both mechanisms.

A possible explanation may be that there still exist some discrepancies between the modeled and real H-radical activities, as H is the sole driver of N_2O decomposition in the colder region of the flame. Other, rather speculative explanations may be that the spin forbidden unimolecular decomposition may play a more significant role than predicted by the mechanism. Also, the improved reaction rates proposed by Janzer et al. [3] based on a sensitivity analysis may still need some adjustment. Perhaps one of the less sensitive reactions may play a more pronounced role or some other decomposition reaction to consume N_2O may be missing altogether. Further dedicated experiments are needed to narrow down the reason for the observed discrepancies.

A rate of production analysis with respect to total carbon flow at 3.5 mm HAB and over the flame can be found in the SI (Figs. S1 and S3). Initial fuel decomposition mainly takes place via hydrogen addition to form ethyl radicals (C_2H_5) (R6) and by hydrogen abstraction through H and OH radicals to form vinyl radicals (C_2H_3) (mole fraction data for this radical is included in the SI) (R7 and R8).

$$C_2H_4+H+(M)=C_2H_5+(M) \quad (R6)$$

$$C_2H_4+H=C_2H_3+H_2 \quad (R7)$$

$$C_2H_4+OH=C_2H_3+H_2O \quad (R8)$$

Subsequent steps are the classical hydrogen abstraction and addition reactions followed by β-scissions (cf. Fig. S1). No direct interaction takes place between the fuel and the oxidizer as oxidizer decomposition is solely driven by hydrogen in the zone of high fuel concentration and lower temperatures.

4. Intermediates and minor species

Only few species arising from hydrocarbon nitrogen interactions were observed in the flame. This section concentrates on the important HCN and the isocyanic (HNCO) and fulminic acids (HCNO). Also, we are able to report a measured isomer branching ratio for these compounds, to our knowledge a first for a photoionization laminar flame study and we touch on the model performance for these species. Besides these species only ammonia (NH_3), acetonitrile (CH_3CN), cyanoacetylene (C_3HN) and acrylonitrile (C_3H_3N) were assigned, and their threshold photoelectron spectra and mole fraction profiles can be found in the SI (cf. Figs. S5–S8). Interestingly, NH_3 was the only N_xH_y species detected in the flame, despite their proposed importance and activity in N_2O oxidized combustion [6,8].

Hydrogen cyanide (HCN) is an intermediate species that occurs in high concentration in the flame and is generally an important species for nitrogen interactions in combustion [25]. The formation of HCN is significant for the flame conditions reported here and the concentration of HCN is relatively high at a peak mole fraction of ca. $1.5 \bullet 10^{-2}$. The mole fraction (i.e., sum of HNC and HCN) profile displayed in Fig. 5 shows a narrow and steep progression and occurrence of HCN up to a HAB of 10 mm.

The extent of the profile coincides with the region of highest temperatures but reaches well beyond the point of full fuel and oxidizer consumption (ca. 5 mm HAB). Significantly, in comparison to the models, despite the limited agreement regarding the mole fraction, M2 shows substantial improvement of the profile shape and HABs of occurrence. Both points of onset and complete consumption of this species agree excellently with the enhanced model. M1 on the other hand predicts a much broader profile and HCN to be a significant contributor to the exhaust species. Hence, HCN was picked as a model species for the discussion of the performance of M1 and M2 respectively.

A ROP analysis at the point of highest concentration of HCN (i.e. 5 mm HAB) shows that the most significant contributor to HCN production is the reaction of N_2O with CH (R9). This reaction is analog (albeit not energetically) to the originally proposed prompt NO formation reaction. The second isomer hydrogen isocyanide (HNC) is mainly formed by reaction R10 at 3.5 mm HAB.

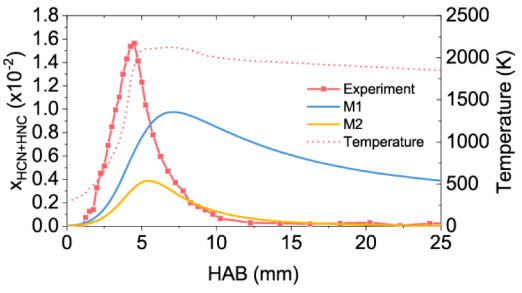

Fig. 5. Experimental mole fraction profiles of the sum of HCN and HNC (symbols) in comparison to modeling results (lines).

$CH+N_2O=HCN+NO$ (R9)

$HCN+H=HNC+H$ (R10)

The measured decrease of HCN concentration below the detection threshold at higher HABs is significant evidence for the performance of M2 over M1. For the investigated conditions and the developed models, HCN shows the significant influence of the N_2O decomposition rates on the overall reaction network. At higher HABs (i.e., evaluated at 8 mm HAB), a major reaction for the consumption of HCN is its reaction with H to form H_2 and CN (R11).

$HCN+H=CN+H_2$ (R11)

This observation may imply that the increasing H radical concentration in the zone where N_2O is fully decomposed (cf. Fig. 3) is a contributor to the total consumption of HCN. Model M1 significantly underestimates H concentration (cf. Fig. 3) in the post oxidizer decomposition region of the flame, while overestimating HCN concentration in this zone, further corroborating this notion.

HNCO (isocyanic acid) and its isomers HOCN (cyanic acid) and HCNO (fulminic acid) play an important role in combustion reactions involving nitrogen interactions [26]. Their signal appears at a mass-to-charge ratio (m/z) of 43 in the mass spectrum obtained from the flame. It was successfully and securely assigned to the HNCO and HCNO isomers by their measured photoelectron spectra and by comparing the photoion (PI) spectrum to known adiabatic ionization energies [27–29]. The result is shown in Fig. 6. The photoelectron reference spectra match the measured mass-selective threshold photoelectron spectra (ms-TPES) of HNCO and HCNO excellently.

No sign of the HOCN isomer was found. This may be attributed to the fact that HOCN is produced at a substantially lower rate than the other isomers. Another explanation for the absence of HOCN might be fast tautomerization to HNCO due to wall collisions during the sampling process [30]. Hot quartz surfaces can accelerate those tautomerizations [31]. The photoion spectrum shows a similar situation. Two steep rises at ca. 10.8 eV and 11.6 eV corresponding with the adiabatic ionization energies of HCNO and HNCO [29] are visible in the top panel of Fig. 6.

The comparison of the measured and modeled mole fraction profiles for the isocyanic and fulminic acids are displayed in Fig. 7. M1 shows an

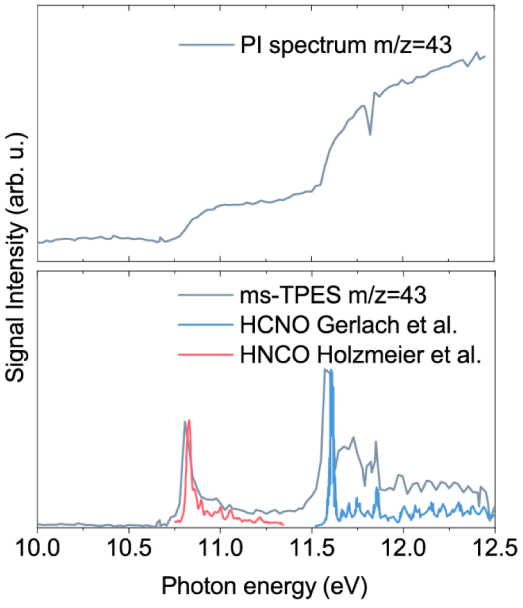

Fig. 6. PI spectrum (top panel) and ms-TPES of $m/z = 43$ with the assignment by literature spectra to identify fulminic (HCNO) and isocyanic (HNCO) acids (bottom panel).

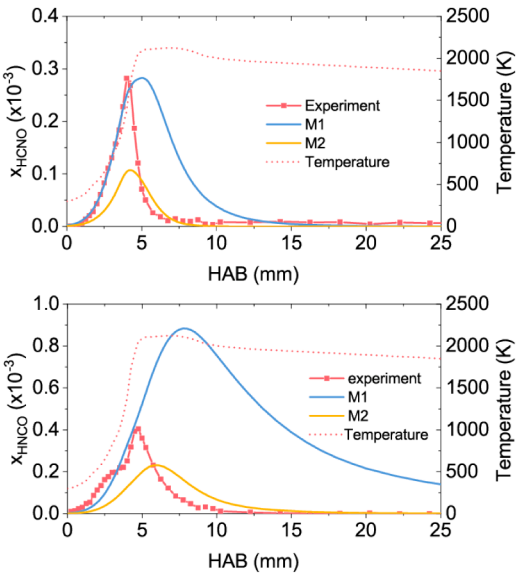

Fig. 7. Mole fraction profiles of HCNO (top panel) and HNCO (bottom panel) in comparison to modeling results of M1 and M2.

unsatisfactory result in the profile width. Here again, similar to the observation made in the case of HCN, the profile becomes too broad with M1. Also, HNCO is predicted as a substantial exhaust gas species, which can be ruled out, since it is below the detection threshold at HAB larger than 10 mm. M2 reproduces the profile shape, width and position well. Concentrations are well within the measurement uncertainties of a factor 2 to 4 for the quantification of species with unknown absolute photoionization cross sections [32] and is a substantial improvement over the base mechanism M1.

In the hot reaction zone at a HAB of 3.5 mm, a ROP analysis shows that HNCO is mostly produced by reactions R12 and R13, while HCNO is mostly produced by R14.

$NH_2+CO = HNCO+H$ (R12)

$HNC+OH=HNCO+H$ (R13)

$HCCO+NO = HCNO+CO$ (R14)

These results corroborate the notion that initial decomposition directly contributes to these reactions since HCN and NO are both produced in the initial decomposition steps of N_2O (cf. reactions R3 and R10).

The H radical is at play in these reactions, similar to the ones previously discussed. The performance gain of M2 over M1 thus may be explicable by the improvement in the modeling of N_2O decomposition rates and the resulting improvement in the prediction of H concentration (cf. Fig. 3). The high activity of the H radical in this flame and its influence on the overall reaction network is consistent with the findings of Dindi et al. [15] that N_2O oxidized CO flames completely lack radical activity except for O radicals.

The photoionization based analytical technique allows the determination of isomer branching ratios for HNCO and HCNO in a laminar flame for the first time to our knowledge. Table 1 shows the calculated isomer branching ratios for the experiment and models respectively. It was calculated by using the maximum mole fraction (left column) and by integrating the whole mole fraction profile by means of a rolling sum over all concentrations at all HABs (right column). Assuming that the cross sections of the isomers are quite similar due to the similar structure of the molecules, the isomer branching ratio is independent of quantification errors.

The rolling sum shows good agreement with the measurement for both models, while some discrepancies appear in the maximum

Table 1
Isomer branching ratios of HNCO and HCNO.

	Peak conc.	Rolling sum
	Exp.	Exp.
HNCO	0.589	0.672
HCNO	0.411	0.328
	M1	M1
HNCO	0.7577	0.680
HCNO	0.2423	0.320
	M2	M2
HNCO	0.4499	0.657
HCNO	0.5501	0.343

concentration ratio. It is however seen that M2 is much better than M1 in predicting ratios of peak concentrations. Clearly, independent measurements of the isomer ratio are needed to further improve the model predictions and corroborate the findings.

5. Conclusion

We report the detailed flame structure of a C_2H_4 flame oxidized with N_2O with focus on nitrogen-containing species in comparison to a newly developed detailed reaction mechanism. The mechanism contains both hydrocarbon chemistry up to C_6 species and nitrogen interactions up to C_2 species. The base reaction mechanism is enhanced by recently reported decomposition rates for N_2O. The enhanced model performs well and shows very good agreement with the measurements. We show that N_2O decomposition kinetics, albeit only representing the very first step in the unfolding reaction network, have significant influence on the overall speciation in the flame. The enhanced mechanism M2 shows better performance, both, for modeling the decomposition of N_2O as well as for the concentration and profile shape of intermediates.

Despite the active nature of the oxidizer and the high concentrations of reactive nitrogen species like NO, few nitrogenized intermediates were detected. This leads to the conclusion that for reduced mechanism development, the N_2O decomposition kinetics and kinetics of fuel decomposition play the most significant role. Also, H was found to be a highly active radical in the reaction network both in the decomposition of the oxidizer and fuel in reactions with nitrogen intermediates such as HCN.

Novelty and significance statement

The novelty of this research is that we measured a detailed flame structure and are able to present insights into the complex chemical interactions in an N_2O oxidized hydrocarbon (C_2H_4) flame. We also report a substantially improved mechanism including the most recent decomposition rates for N_2O decomposition. The topic is at the intersection of chemistry and engineering, and it is significant because oxidizers like N_2O may become more important in the future, for example, when the reactivity of an oxidation process must be tailored. This work provides validation data for nitrogen interactions with hydrocarbon chemistry in combustion. They play a crucial role in mitigating NO_x emissions and improving combustion processes in advanced space propulsion systems and in any combustion process involving nitrogen interactions and the N_2O mechanism.

Author contributions

- M.H.: Experiment design, measurement of data, data reduction, simulation modeling, writing of the manuscript
- T.B.: Data reduction, simulation modeling, writing of the manuscript
- S.S.: Mechanism development, simulation modeling
- T.K.: Experiment supervision, proofing of the manuscript

Declaration of competing interest

The authors declare that they have no known competing financial interests or personal relationships that could have appeared to influence the work reported in this paper.

Acknowledgements

The experiment was carried out at the VUV beamline of the Swiss Light Source. The authors are thankful for beamtime and expert technical assistance by Patrick Hemberger and Andras Bodi. Funding by the DFG under contract 270672969 and KO4786/2-2 is gratefully acknowledged.

Supplementary materials

Supplementary material associated with this article: Combustion mechanisms, additional figures, mole fraction profiles of measured species. Supplementary material associated with this article can be found, in the online version, at doi:10.1016/j.proci.2024.105683.

References

[1] P. Glarborg, J.A. Miller, B. Ruscic, S.J. Klippenstein, Modeling nitrogen chemistry in combustion, Prog. Energy Combust. Sci. 67 (2018) 31–68.
[2] A.S. Gohardani, J. Stanojev, A. Demairé, K. Anflo, M. Persson, N. Wingborg, C. Nilsson, Green space propulsion: opportunities and prospects, Prog. Aerosp. Sci. 71 (2014) 128–149.
[3] C. Janzer, S. Richter, C. Naumann, T. Methling, Green propellants" as a hydrazine substitute: experimental investigations of ethane/ethene-nitrous oxide mixtures and validation of detailed reaction mechanism, CEAS Sp. J. 14 (2022) 151–159.
[4] S.A. Whitmore, S.N. Chandler, Engineering model for self-pressurizing saturated-N_2O-propellant feed systems, J. Propuls. Power 26 (2010) 706–714.
[5] S.T. Darian, M. Vanpee, A spectroscopic study of the premixed acetylene nitrous oxide flame, Combust. Flame 70 (1987) 65–77.
[6] O.A. Powell, P. Papas, Flame structure measurements of nitric oxide in hydrocarbon-nitrous-oxide flames, J. Propuls. Power 28 (2012) 1052–1059.
[7] M.T. Allen, R.A. Yetter, L. Dryer, Hydrogen/nitrous oxide kinetics-implications of the N_xH_y species, Combust. Flame 112 (1998) 302–311.
[8] O.A. Powell, P. Papas, C.B. Dreyer, Flame structure measurements of NO in premixed hydrogen-nitrous oxide flames, Proc. Combust. Inst. 33 (2011) 1053–1062.
[9] J. Vandooren, M.C. Branch, P.J. Van Tiggelen, Comparisons of the structure of stoichiometric CH4-N2O-Ar and CH4-O2-Ar flames by molecular beam sampling and mass spectrometric analysis, Combust. Flame 90 (1992) 247–258.
[10] S. Zabarnick, A comparison of $CH_4/NO/O_2$ and CH_4/N_2O flames by LIF diagnostics and chemical kinetic modeling, Combust. Sci. Technol. 83 (1992) 115–134.
[11] J. Vandooren, J. Bian, P.J. Van Tiggelen, Comparison of experimental and calculated structures of an ammonia nitric oxide flame. Importance of the NH_2 + NO reaction, Combust. Flame 98 (1994) 402–410.
[12] J. Vandooren, P.J. Van Tiggelen, J.-F. Pauwels, Experimental and modeling studies of a rich $H_2/CO/N_2O/Ar$ flame, Combust. Flame 109 (1997) 647–668.
[13] X. Han, M. Lubrano Lavadera, A.A. Konnov, An experimental and kinetic modeling study on the laminar burning velocity of NH_3+N_2O+air flames, Combust. Flame 228 (2021) 13–28.
[14] D.G.R. Andrews, P. Gray, Combustion of ammonia supported by oxygen, nitrous oxide or nitric oxide: laminar flame propagation at low pressures in binary mixtures, Combust. Flame 8 (1964) 113–126.
[15] H. Dindi, H.-M.- Tsai, M.C. Branch, Combustion mechanism of carbon monoxide-nitrous oxide flames, Combust. Flame 87 (1991) 13–20.
[16] W. Wang, H. Zhang, Laminar burning velocities of C_2H_4/N_2O flames: experimental study and its chemical kinetics mechanism, Combust. Flame 202 (2019) 362–375.
[17] L. Werling, F. Lauck, D. Freudenmann, N. Röcke, H. Ciezki, S. Schlechtriem, Experimental investigation of the flame propagation and flashback behavior of a green propellant consisting of N_2O and C_2H_4, J. Energy Power Eng. 11 (2017) 735–752.
[18] B. Sztáray, K. Voronova, K.G. Torma, K.J. Covert, A. Bodi, P. Hemberger, T. Gerber, D.L. Osborn, CRF-PEPICO: double velocity map imaging photoelectron photoion coincidence spectroscopy for reaction kinetics studies, J. Chem. Phys. 147 (2017) 013944.
[19] P. Oßwald, P. Hemberger, T. Bierkandt, E. Akyildiz, M. Köhler, A. Bodi, T. Gerber, T. Kasper, In *situ* flame chemistry tracing by imaging photoelectron photoion coincidence spectroscopy, Rev. Sci. Instrum. 85 (2014) 025101.
[20] U. Struckmeier, P. Oßwald, T. KAsper, L. Böhling, M. Heusing, M. Köhler, A. Brockhinke, K. Kohse-Höinghaus, Sampling probe influences on temperature and species concentrations in molecular beam mass spectroscopic investigations of flat premixed low-pressure flames, Zeitschrift fur Phys. Chemie 223 (2009) 503–537.

[21] C.W. Zhou, et al., An experimental and chemical kinetic modeling study of 1,3-butadiene combustion: ignition delay time and laminar flame speed measurements, Combust. Flame 197 (2018) 423–438.
[22] A. Karabeyoglu, J. Dyer, J. Stevens, B. Cantwell, Modeling of N_2O decomposition events, in: 44th AIAA/ASME/SAE/ASEE Joint Propulsion Conference and Exhibit, 2008, p. 4933.
[23] M. Hoener, T. Kasper, Nitrous acid in high-pressure oxidation of CH_4 doped with nitric oxide: challenges in the isomer-selective detection and quantification of an elusive intermediate, Combust. Flame 243 (2022) 112096.
[24] S.J. Klippenstein, M. Pfeifle, A.W. Jasper, P. Glarborg, Theory and modeling of relevance to prompt-NO formation at high pressure, Combust. Flame 195 (2018) 3–17.
[25] Z.W. Sun, Z.S. Li, A.A. Konnov, M. Aldén, Quantitative HCN measurements in CH_4/N_2O/O_2/N_2 flames using mid-infrared polarization spectroscopy, Combust. Flame 158 (2011) 1898–1904.
[26] K. Kohse-Höinghaus, P. Oßwald, T.A. Cool, T. Kasper, N. Hansen, F. Qi, C. K. Westbrook, P.R. Westmoreland, Biofuel combustion chemistry: from ethanol to biodiesel, Angew. Chemie - Int. Ed. 49 (2010) 3572–3597.
[27] M. Gerlach, et al., Photoelectron spectroscopy and dissociative photoionization of fulminic acid, HCNO, J. Chem. Phys. 158 (2023) 134303.
[28] F. Holzmeier, et al., Threshold photoelectron spectroscopy of unstable N-containing compounds: resolution of ΔK subbands in $HNCO^+$ and vibrational resolution in NCO^+, J. Chem. Phys. 142 (2015) 184306.
[29] P. Linstrom and W.G. Mallard, NIST Chemistry WebBook, NIST Standard Reference Database Number 69, National Institute of Standards and Technology, Gaithersburg MD, 20899.
[30] D. Bégué, W. Lafargue-Dit-Hauret, A. Dargelos, C. Wentrup, CHNO - Formylnitrene, Cyanic, Isocyanic, Fulminic, and Isofulminic acids and their interrelationships at DFT and CASPT2 levels of theory, J. Phys. Chem. A 127 (2023) 9088–9097.
[31] C. Wentrup, Flash vacuum pyrolysis: techniques and reactions, Angew. Chemie - Int. Ed. 56 (2017) 14808–14835.
[32] N. Hansen, T.A. Cool, P.R. Westmoreland, K. Kohse-Höinghaus, Recent contributions of flame-sampling molecular-beam mass spectrometry to a fundamental understanding of combustion chemistry, Prog. Energy Combust. Sci. 35 (2009) 168–191.